# Diffractive Dijet Production in pA vs eA

- Breakdown of Factorization in pp Diffraction
- Renormalized Pomeron Model
- Inelastic Shadowing in pA
- Diffractive Dijet Production in pA vs eA

Stephen E. Vance
Brookhaven National Laboratory
in collaboration with
Dima Kharzeev

Quark Matter
January 19, 2001

# I. Deep Inelastic Scattering

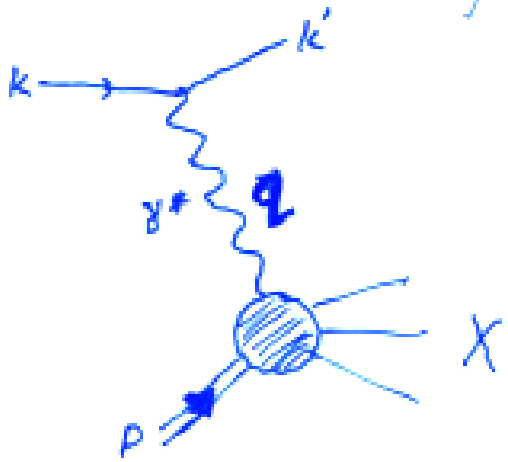


$$x = \frac{Q^2}{2P \cdot q}$$

# II. Diffractive Scattering

(~10% of virtual photon-proton cross section)

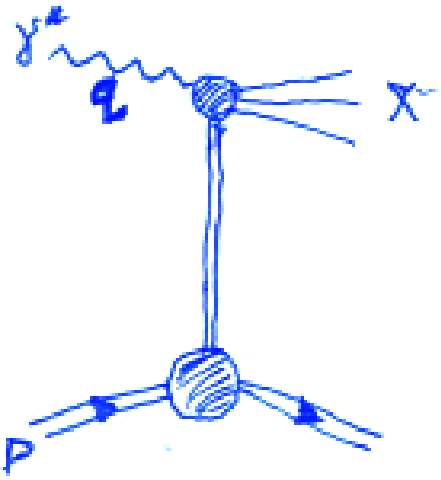


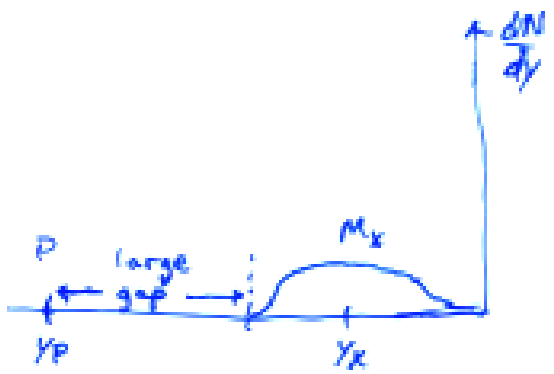

# Breakdown of Factorization

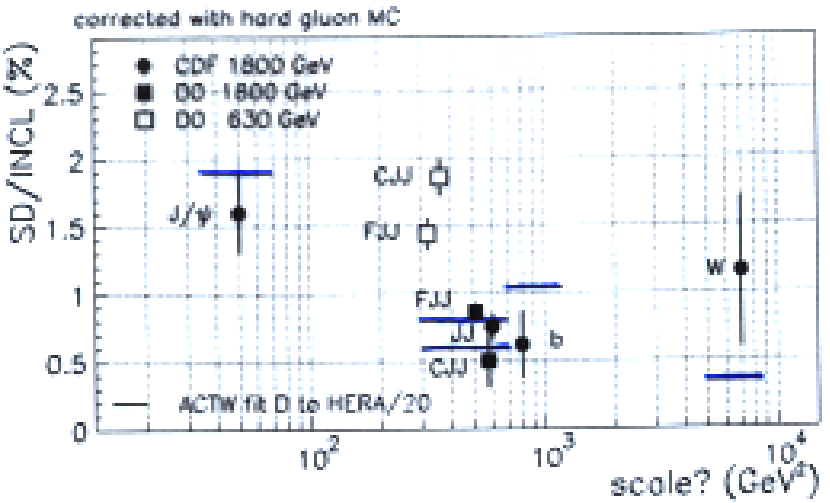


Ref: H. Abramowicz hep-ph/0001054

— Expectation 20

Figure 10: Ratio of single diffraction to inclusive production in $p\bar{p}$, SD/INCL, as a function of the approximate hard scale in the process. JJ stands for two jet production while C and F stand for forward and central production. Horizontal bars are expectations obtained using the ACTW parameterization, fit D [46], scaled down by factor 20.

- Using diffractive parton distribution functions (from HERA), jet production in single diffractive compared to inclusive production in $p\bar{p}$ is overestimated by a factor of 20!

- QCD factorization breaks down in hadron collisions due to absorptive corrections


[g probe in $p\bar{p}$ reduces large rapidity gap events due to strong interactions with everything]

# Renormalized Pomeron Model

K. Goulianos and J. Montanha (1999), hep-ph/9805496

- **Single Diffractive Cross Section**

$$\frac{d^2\sigma^{diff}}{dM^2dt} = \underbrace{\frac{\beta^2_{Ppp}(t)}{16\pi}\left(\frac{M^2}{s}\right)^{1-2\alpha_P(t)}}_{f_{P/p}(M^2/s,t)} \underbrace{\left[\beta_{Ppp}(0)g(t)\left(\frac{M^2}{s_0}\right)^{\alpha_P(0)-1}\right]}_{\sigma_T^{Pp}(s')}$$


- **Integrated SD Cross Section Violates Unitarity:**

$$\sigma_{SD}(s) \sim s^{2\epsilon} \quad \text{while} \quad \sigma_T(s) \sim s^{\epsilon}$$

where $\alpha_P = 1 + \epsilon + \alpha' t$ and $\epsilon = 0.08 - 0.10$

- **Renormalize the Flux Factor**

Interpret $f_{P/p}(M^2/s,t)$ as a the probability density.

$$f_N(M^2/s,t) = \begin{cases} f_{P/p}(M^2/s,t) & \text{if } N(s) < 1 \\ \frac{1}{N(s)} f_{P/p}(M^2/s,t) & \text{if } N(s) > 1 \end{cases}$$

where

$$N(s) = \int_{1.5/s}^{0.1}\int_{-\infty}^{0} f_{P/p}(M^2/s,t)\; d(M^2/s)dt$$

The result is

$$\lim_{s\to\infty} \sigma^N_{sd}(s) = const$$

- **Renormalized SD cross section**

$$\frac{d^2\sigma^{diff}}{dM^2dt} = f_N(M^2/s,t)\; \sigma_T^{Pp}(s')$$

# Total single diffraction cross section for $p(\bar{p}) + p \to p(\bar{p}) + X$ (comparison with theoretical predictions)

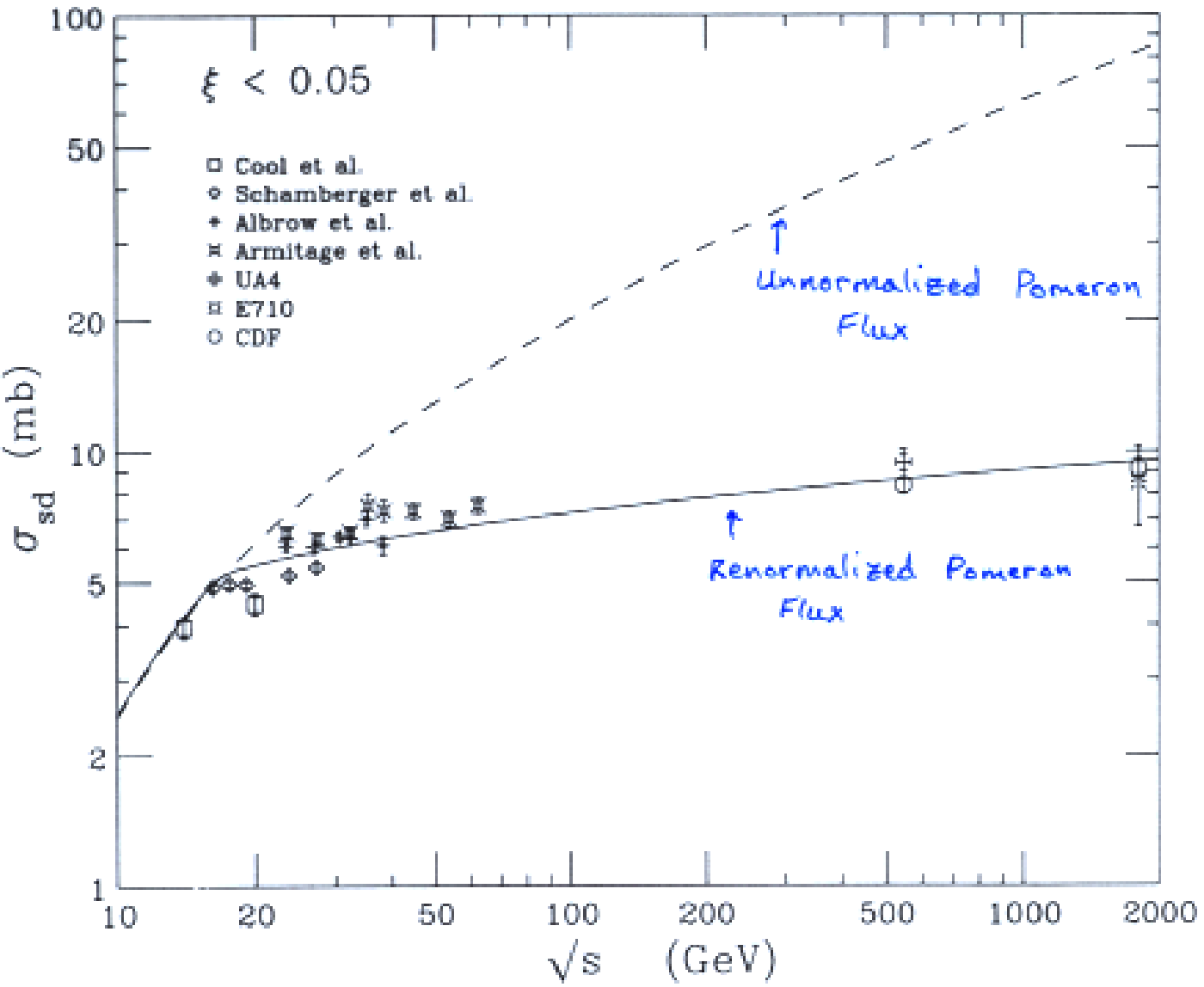


Figures 12: Total single diffraction cross sections for $p(\bar{p}) + p \to p(\bar{p}) + X$ versus $\sqrt{s}$ compared with triple-pomeron predictions based (a) on pomeron pole dominance in standard Regge theory (dashed line) and (b) on the renormalized pomeron flux model [4] (solid line). The cross sections were corrected for effects due to extrapolations in $t$, as discussed in the text. The errors shown are statistical; typical systematic uncertainties for each experiment are of $\mathcal{O}(10\%)$.

Ref: Goulianos & Montanha (1998) hep-ph/9805496

# Inelastic Shadowing

- **Scattering Diagrams**

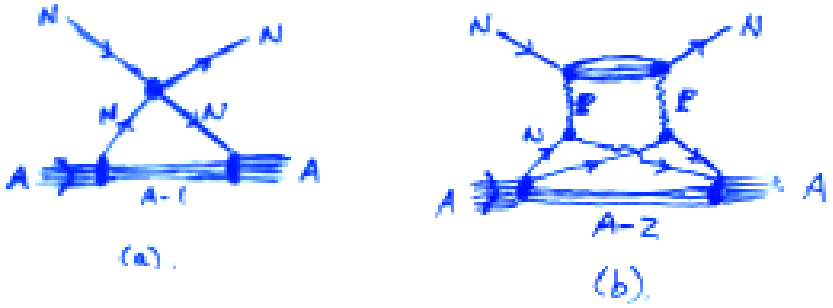


- Total pA Cross Section

$$\sigma_{pA} = A\sigma_{pN} + \delta\sigma_{pA},$$

where

$$\delta\sigma_{pA} = -8\pi \int d^2b \int_{-\infty}^{\infty} dz_1 \int_{z_1}^{\infty} dz_2 \;\; \rho_A(\vec{b}, z_1)\rho_A(\vec{b}, z_2) \times \int_{M_0^2}^{0.1s} dM^2 \cos\left((z_1 - z_2)/\lambda\right) \left.\frac{d^2\sigma_{pp}^{diff}}{dM^2 dt}\right|_{t=0} e^{-\frac{\sigma_{pN}}{2}\int_{z_1}^{z_2} dz\, \rho_A(\vec{b}, z)}$$

the factors

$$\lambda = m_p(M^2 - m_p^2)/s, \qquad \frac{d^2\sigma_{pp}^{diff}}{dM^2 dt} \sim \frac{s^{2\epsilon}}{(M^2)^{(1+\epsilon)}}$$

and throughout

$$\rho_A(\vec{r}) = A\left(\frac{3}{2\pi\langle r^2\rangle_A}\right)^{3/2} \exp\left(-\frac{3\vec{r}^2}{2\langle r^2\rangle_A}\right)$$

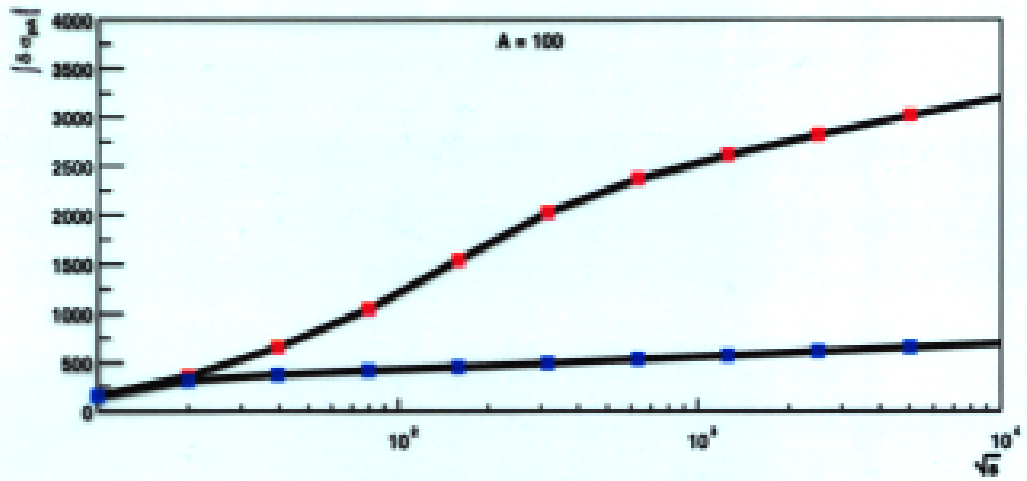


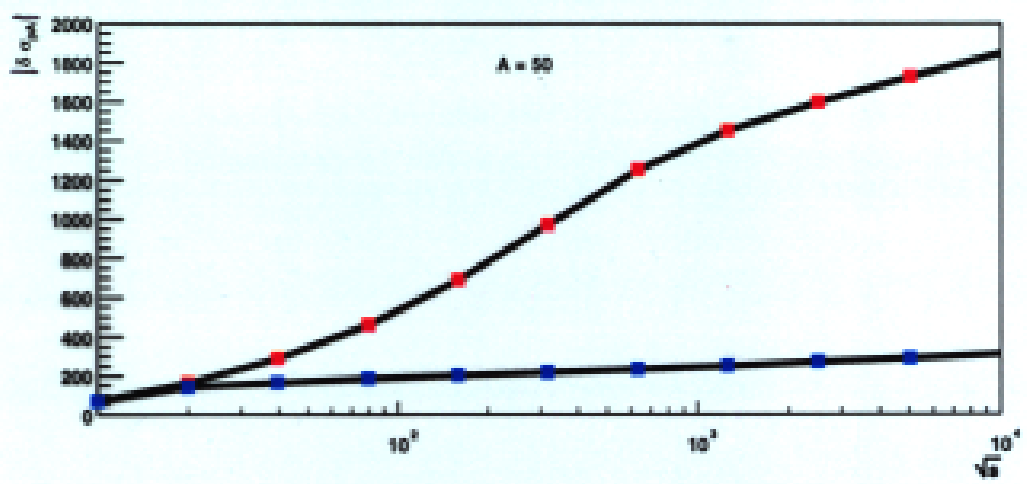


Unnormalized PPF

Renormalized PPF

$$\sigma_{pA} = A\sigma_{pp} - |S\sigma_{pA}|$$

# Shadowing

- **Shadowing**

$$R(x,Q^2) = \frac{F_2^A(x,Q^2)}{F_2^N(x,Q^2)} = \frac{\sigma_{\gamma^* A}}{A\sigma_{\gamma^* N}}$$

- **Scattering Diagrams**

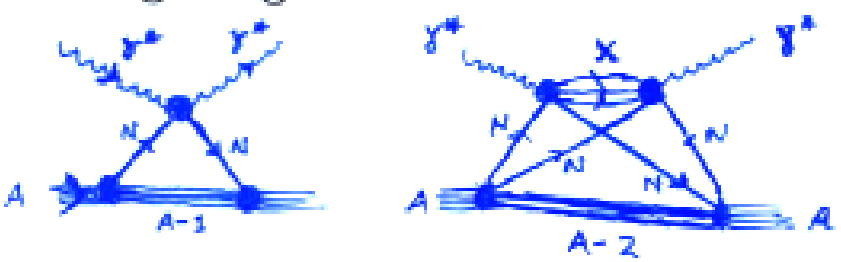


- **Total pA Cross Section**

$$\sigma_{\gamma^* A} = A\sigma_{\gamma^* N} + \delta\sigma_{\gamma^* A},$$

where

$$\delta\sigma_{\gamma^* A} = -8\pi \int d^2b \int_{-\infty}^{\infty} dz_1 \int_{z_1}^{\infty} dz_2 \;\; \rho_A(\vec{b},z_1)\rho_A(\vec{b},z_2) \times \int_{M_0^2}^{W^2} dM^2 \cos\left((z_1-z_2)/\lambda\right) \left.\frac{d^2\sigma^{diff}_{\gamma^* N}}{dM^2 dt}\right|_{t\approx 0}$$

where $1/\lambda = mx(1+M^2/Q^2)$ and $W \approx Q/\sqrt{x}$

- **Contributions to the diffractive cross section**

1. $\rho, \omega, \phi$: $\left.\frac{d^2\sigma^{diff}_{\gamma^* N}}{dM^2 dt}\right|_{t\approx 0} = \frac{\alpha}{4}\frac{M^2}{M^2+Q^2}\sigma^2_{XN}\left(\frac{m_v}{g_v}\right)^2 \delta(M^2-m_v^2)$

2. $q\bar{q}$ Continuum: $\left.\frac{d^2\sigma^{diff}_{\gamma^* N}}{dM^2 dt}\right|_{t\approx 0} = C\frac{(W^2)^{2(\alpha_P(0)-1)}}{(M^2)^{\alpha_P(0)}}$

# Nuclear Shadowing

Ref: Piller & Weise
Phys Rept 330 (2000) 1

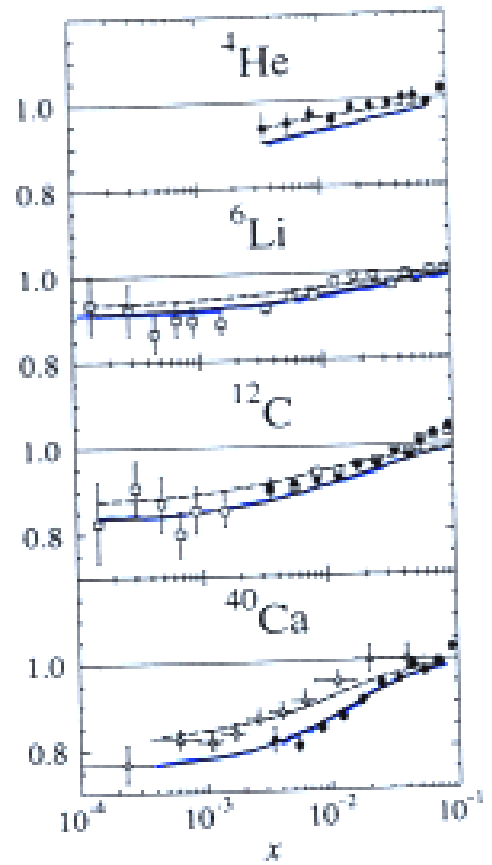


Fig. 5.10. Results from Ref.[169] for the shadowing in He, Li, C, and Ca compared to experimental data from NMC (dots and squares) [71,75] and FNAL (triangles) [77]. The dashed curves show the shadowing caused by the vector mesons $\rho$, $\omega$ and $\phi$ only, the solid curves are the results including the $q\bar{q}$ continuum.

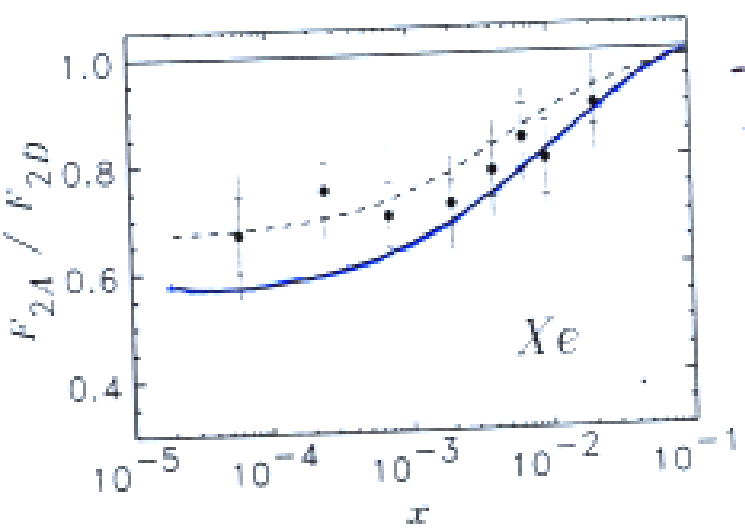


Fig. 5.12. Shadowing in Xe. Details of the calculation are given in Ref.[154]. The dashed curve shows the contribution of vector mesons $\rho$, $\omega$ and $\phi$, while the solid curve includes pomeron exchange. The data are from the E665 collaboration [76].

# Diffractive Cross Section

D. Kharzeev and S.E. Vance, in preparation

- **Total $\gamma^* A$ Cross Section**

$$\sigma^{tot}_{\gamma^* A} = 2 \int d^2b \left[ 1 - e^{\left( -\frac{1}{2} \sigma^{tot}_{\gamma^* p} T(b) \right)} \right] + \delta\sigma_{\gamma^* A},$$

where

$$\delta\sigma^{tot}_{\gamma^* A} = -4\pi \int d^2b \, e^{\left( -\frac{1}{2} \sigma^{tot}_{\gamma^* p} T(b) \right)} \int dM^2 \, \tilde{T}^2(b, M^2) \frac{d\sigma_{\gamma^* p}}{dM^2 dt}\Big|_{t=0},$$

$$T(b) = \int_{-\infty}^{\infty} dz \rho(\vec{b}, z) \quad \text{and} \quad \tilde{T}(b, M^2) = \int_{-\infty}^{\infty} dz \rho(\vec{b}, z) e^{iz/\lambda}$$

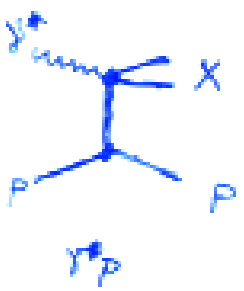


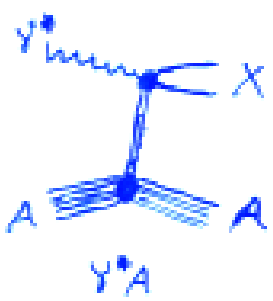


- **Diffractive $\gamma^* A$ Cross Section**

$$\sigma^{diff}_{\gamma^* A} = \sum_l \sigma(\gamma^* A \to h_l A) - \sigma^{el}_{\gamma^* A}$$

# Diffractive Cross Section

D. Kharzeev and S.E. Vance, in preparation

- **Total diffractive cross section**

$$\sigma^{diff}_{\gamma^* A} = 4\pi \int d^2b \int dM^2 \, \tilde{T}^2(b, M^2) \, e^{-\sigma^{tot}_{\gamma^* p} T(b)} \left. \frac{d\sigma_{\gamma^* p}}{dM^2 dt} \right|_{t=0},$$

  where throughout $\sigma^{tot}_{\gamma^* p} = 28.73\text{mb}$

- **Differential diffractive cross section**

$$\frac{d\sigma^{diff}_{\gamma^* A}}{dM^2} = 4\pi \left. \frac{d\sigma_{\gamma^* p}}{dM^2 dt} \right|_{t=0} \int d^2b \, \tilde{T}^2(b, M^2) \, e^{-\sigma^{tot}_{\gamma^* p} T(b)}$$

- **Ratio of $\gamma^* A$ to $\gamma^* p$**

$$\begin{aligned} R(M^2) &= \frac{d\sigma^{diff}_{\gamma^* A}}{dM^2} \Big/ A \frac{d\sigma^{diff}_{\gamma^* p}}{dM^2} \\ &= \frac{4\pi}{A} \int d^2b \, \tilde{T}^2(b, M^2) \, e^{-\sigma^{tot}_{\gamma^* p} T(b)} \end{aligned}$$

- **pA**

  The same formulas apply with the following changes

$$\frac{d\sigma^{diff}_{\gamma^* p}}{dM^2} \to \frac{d\sigma^{diff}_{pp}}{dM^2} \quad \text{and} \quad \sigma^{tot}_{\gamma^* p} \to \sigma^{tot}_{pp}$$

  Note: $\sigma^{tot}_{pp} > \sigma^{tot}_{\gamma^* p}$

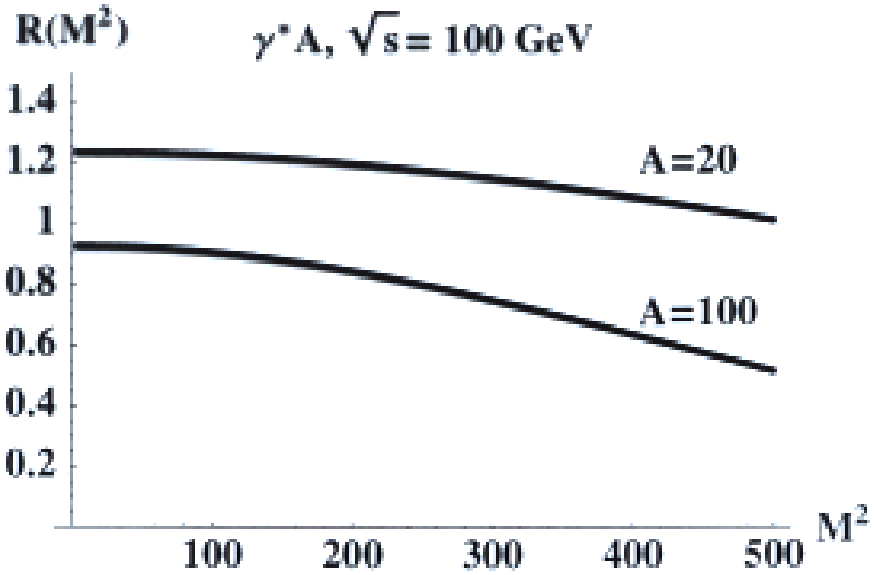
R(M²)
γ*A, √s = 100 GeV
1.4
1.2
1
0.8
0.6
0.4
0.2
A=20
A=100
100
200
300
400
500
M²

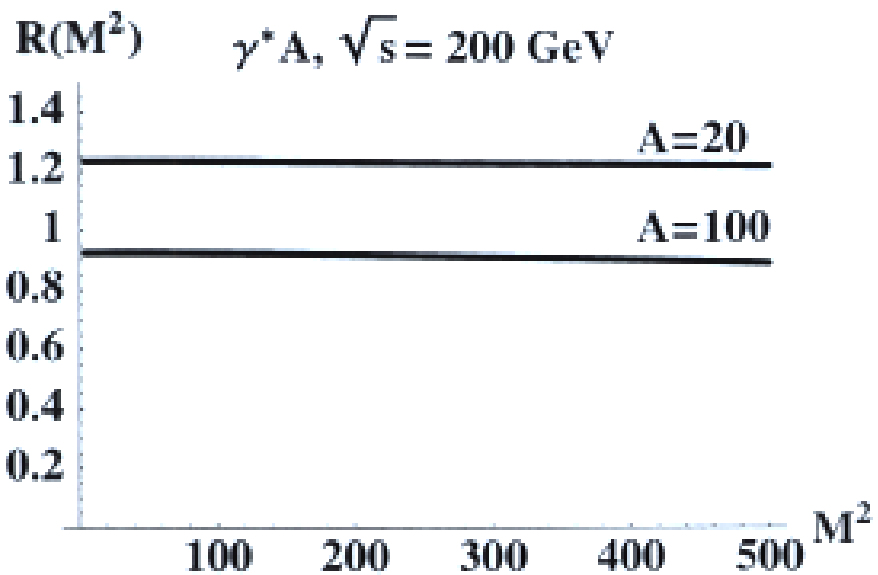
R(M²)
γ*A, √s = 200 GeV
1.4
1.2
1
0.8
0.6
0.4
0.2
A=20
A=100
100
200
300
400
500
M²

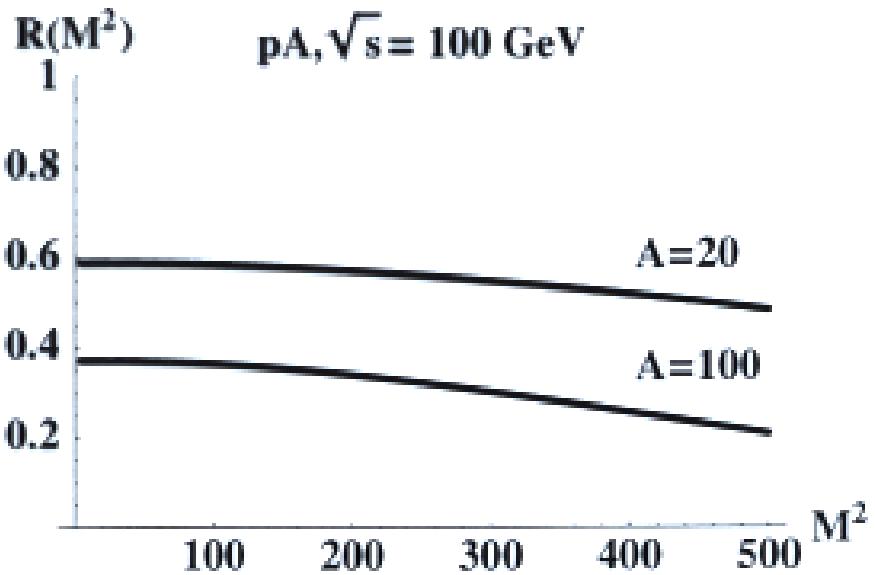
R(M²)
pA, √s = 100 GeV
1
0.8
0.6
0.4
0.2
A=20
A=100
100
200
300
400
500
M²

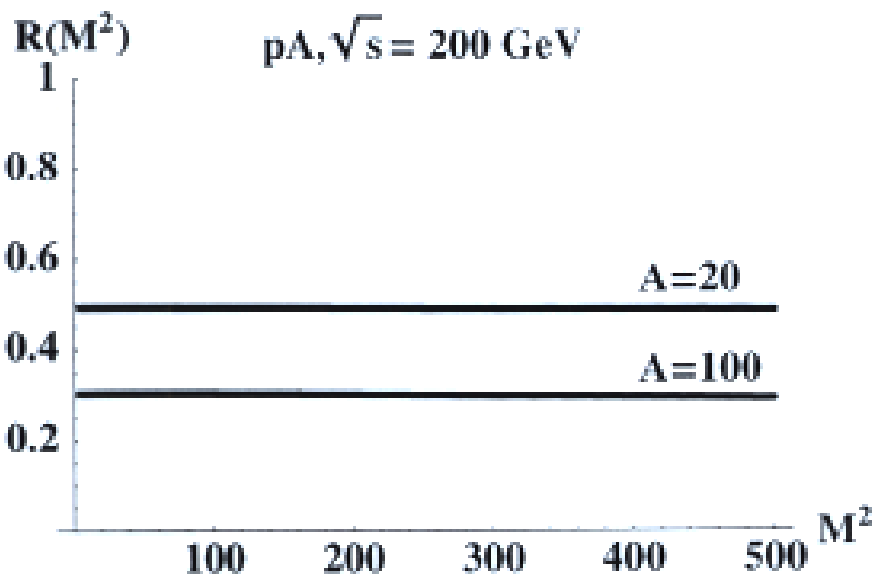
R(M²)
pA, √s = 200 GeV
1
0.8
0.6
0.4
0.2
A=20
A=100
100
200
300
400
500
M²

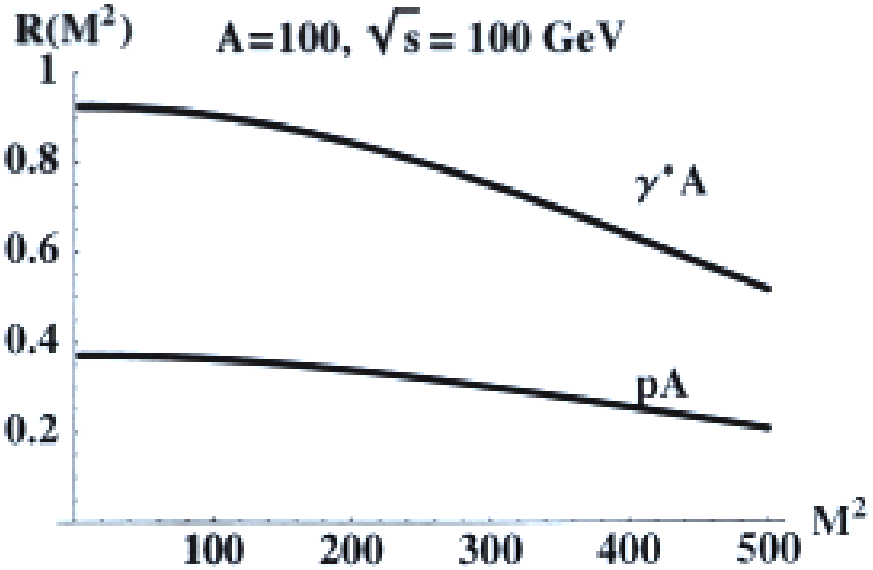
R(M²)
A=100, √s = 100 GeV
1
0.8
0.6
0.4
0.2
γ*A
pA
100
200
300
400
500
M²

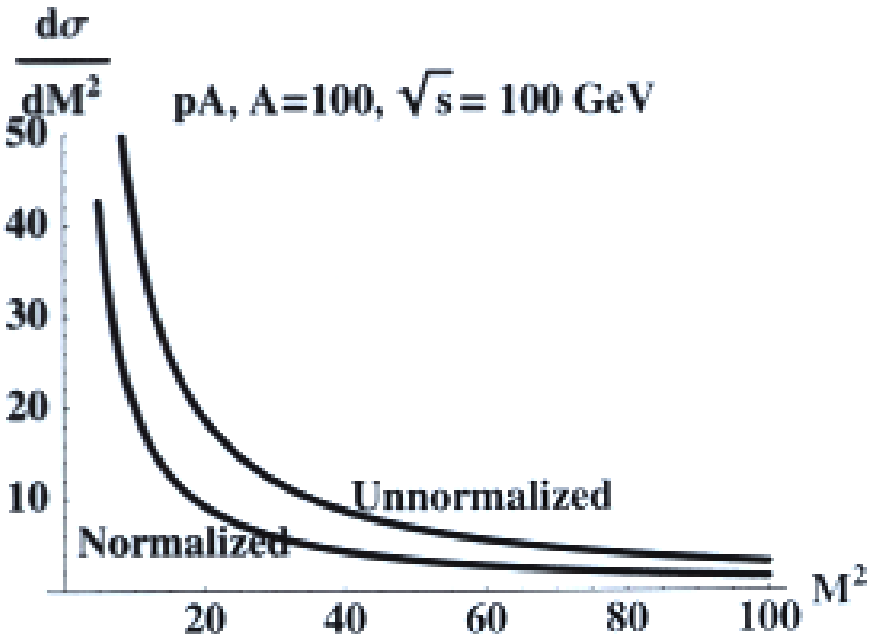
dσ
dM²
pA, A=100, √s = 100 GeV
50
40
30
20
10
Unnormalized
Normalized
20
40
60
80
100
M²

# Conclusions

1. Including absorptive corrections or shadowing effects or screening corrections is important for pp diffractive and pA interactions

   (a) The total cross section for $pA$ interactions becomes larger than previously expected.

   (b) The diffractive cross sections $\frac{d\sigma_{pA}^{diff}}{dM^2}$ is smaller than previously expected.

2. The ratio of diffractive $pp$ and $pA$ cross sections and the ratio of diffractive $\gamma^* p$ and $\gamma^* A$ cross sections differ mainly through the total cross section. This reflects the color state of the probe.

3. Future studies: Study contributions from $n > 2$ collisions